Evolution Mechanism and Application of Miscible Zone in CO_2 Flooding

Ke Zhang[1,2], *Yaoze* Cheng[1,2], *Yu* Zhang[1,2], *Weifeng* Lv[1,2*], *Lin* Jiang[1,2], *Ruisi* Wang[3] , *Tiyao* Zhou[1,2], *Yuhao* Mei[4,5], and *Wang* Zhang[6]

[1]Research Institute of Petroleum Exploration and Development, PetroChina, 100083 Beijing, China
[2]State Key Laboratory of Enhanced Oil and Gas Recovery, 100083 Beijing, China
[3]Huabei Oilfield Exploration & Development Research Institute, PetroChina, 062552 Renqiu Hebei, China
[4]School of Engineering Science, University of Chinese Academy of Sciences, 100049 Beijing, China
[5]Institute of Porous Flow and Fluid Mechanics, Chinese Academy of Sciences, 065007 Langfang Hebei, China
[6]Institute of Geology and Geophysics, Chinese Academy of Sciences, 100029 Beijing, China

Abstract. The miscible zone and degree of miscibility during CO_2 flooding have a significant impact on the development performance of low-permeability, ultra-low-permeability, and unconventional reservoirs. At present, a systematic evaluation method and unified understanding of the miscible zone and degree of miscibility have not yet been established. In this study, an integrated minimum miscibility pressure (MMP) evaluation system, a CO_2 flooding evaluation system, and a CT onsite-scanning oil-gas interface quantitative characterization and evaluation system were employed to comprehensively investigate the CO_2-crude oil MMP, leading and trailing edges of miscible zone, miscible zone scale variation patterns, phase-type characterization within the miscible zone, and the conceptual framework regarding the degree of miscibility. Results indicate that MMP can be accurately determined by integrating the advantage of timesaving of the vanishing interfacial tension, rising bubble, and capillary rising methods with the high accuracy of the slim tube test. The onset of the leading edge of the miscible zone can be determined by the detection of injected CO_2 at the production end, while the trailing edge of that can be identified by a sharp positive slope change in gas-oil ratio and a remarkable increase in C_2-C_{15} components in the produced oil. The region between the leading and trailing edges is defined as the miscible zone. It was clarified that five distinct oil-gas fluid types were identified during CO_2 flooding, and a multi-phase interval identification standard for miscible zone characterization was established. A new definition and calculation method for the degree of miscibility, which incorporates both immiscible and miscible flooding stages, was proposed, enabling universal miscibility evaluation across different reservoir conditions. Furthermore, a mathematical model for CO_2 flooding was also constructed by coupling phase behaviour and fluid flow in porous media. The simulation results closely matched the field production data, which verified the model's reliability. This study establishes a theoretical basis for miscible zone regulation and provides essential technical support for the development of integrated control technologies aimed at enhancing oil recovery.

1 Introduction

In recent years, CO_2 enhanced oil recovery (CO_2-EOR), as a greenhouse gas sequestration technology, has gained global research attention and numerous field applications [1-17]. CO_2 is a high-efficiency oil-displacing agent. After CO_2 is injected into the reservoir, it reduces crude oil viscosity, dissolves and erodes formation to expand seepage channels, and supplements formation energy [18-20]. With technological advances, CO_2 becomes fully miscible with crude oil when the injection pressure reaches the minimum miscibility pressure (MMP), thereby lowering both interfacial tension （IFT）and capillary force to zero. This contributes to an oil displacement efficiency over 90% and substantially improves hydrocarbon recovery [21-24]. During CO_2 miscible flooding, a transition zone is formed by multiple contacts between CO_2 and crude oil, which is defined as the miscible zone [25-26]. Currently, CO_2 miscible flooding studies mainly focus on MMP determination, boundary characterization and migration patterns of the miscible zone, and the evaluation of the degree of miscibility (MD).

Experimental investigation and numerical simulation are the two main methods to study the characterization of the miscible zone. Experiments are widely used to determine MMP, with main approaches including the slim-tube method and the vanish interfacial tension (VIT) method. The slim-tube method relies on a homogeneous one-dimensional physical model; its experimental

* Corresponding author: lweifeng@petrochina.com.cn

schemes can be adjusted by inner diameter and length of the tube, particle size of the packed sand in the tube, and displacement rate, while eliminating interference from viscous fingering, high mobility ratio, and significant reservoir heterogeneity is essential. Su et al. [27] reported that MMP declines with increasing slim-tube length and tends to stabilize after a critical value. Liu et al. [28] found the MMP error between empirical formulas and slim-tube tests is about 10%. However, slim-tube experiments are limited by high complexity and time consumption. The VIT method identifies oil-gas miscibility by finding the relationship between IFT and pressure [29]. ORR et al. [30] revealed MMP rises linearly with increasing temperature, with a growing slope corresponding to higher alkane carbon numbers, though this method fails to acquire accurate data for fully miscible systems. For miscible zone characterization, Cai et al. [31] used NMR to distinguish miscible/immiscible states and set the CO_2 concentration of 52.6 mol% as the miscible zone leading edge. Xin et al. [32] divided displacement stages into non-breakthrough, breakthrough, and massive breakthrough according to CO_2 concentration. In terms of MD, slim-tube tests by Luo et al. [33] indicated that higher miscibility improves recovery efficiency and increases heavy component proportion in produced fluids. Yang et al. [34] combined PVT tests and slim-tube experiments, confirming that immiscible flooding could cause heavy distillate retention and impair reservoir development.

Numerical simulation is another key method for miscible flooding research. For miscible zone boundary identification, Li et al. [35] defined the miscible zone by critical viscosity and IFT values via simulation. Bo et al. [36] delineated the miscible zone and its leading edge by superimposing formation pressure and CO_2 concentration distributions. Numerical simulation also reveals migration rules of miscible zone: sweep efficiency and dimensionless area grow linearly before miscible front breakthrough, followed by a peak and decline in dimensionless width and accelerated viscous fingering growth; after breakthrough, sweep efficiency growth slows down, and related parameters gradually stabilize [37-38]. Increasing differential pressure helps maintain the stability of the miscible zone and enhances oil recovery [39]. Li et al. [40] used a numerical model of miscible flooding to prove that the miscible zone migrates toward production wells with CO_2 injection. It can be concluded that weak adsorption of CO_2, high CO_2 concentration of the injected gas, and large reservoir porosity can accelerate mass transfer and diffusion effects, resulting in the increase in the miscible zone.

In summary, the unified criteria for determining the leading and trailing edges of the miscible zone remain unclear. Research on the miscible zone phase behaviour, its formation mechanism, and experimental-scale MD characterization remains insufficient. In this paper, MMP evaluation methods were first reviewed. Based on a long one-dimensional physical model, CO_2 miscible flooding experiments were performed, and the miscible zone boundaries were redefined. Combined with CT high-pressure cell tests, the variation law of the miscible zone is clarified, and a classification method was established to identify the fluid types within the miscible zone. A mathematical model of the oil-gas miscible zone was further constructed and verified with data obtained from XH Oilfield. This study provides theoretical and technical support for subsequent miscible zone studies.

2 Study on Phase Behaviour Characteristics and Miscibility of CO_2-Crude Oil Systems

2.1 Basic Physical Properties of Crude Oil

The dead oil sample was gained from XH block, and the composition was determined via Agilent 8890 gas chromatography. The molar composition of the oil was as follows: 4.85 mol% of C_4–C_5, 82.57 mol% of C_6–C_{10}, and 12.19 mol% of C_{11+}. The gas composition from the single flash test is presented in Table 1. CO_2 used to prepare live oil in this study was industrial grade with purity over 99%.

Table 1. Composition of Single Flashed Gas.

Component	Mol,%
CO_2	4.533
N_2	1.020
C_1	90.580
C_2	0.305
C_3	0.272
iC_4	0.543
nC_4	1.021
iC_5	1.008
nC_5	0.714
C_6	0.003
C_7	0.001

2.2 Evaluation of MMP for CO_2-Crude Oil System

Currently, the slim-tube experiment is the global key method for measuring MMP. Other common MMP testing methods include bubble rising, VIT, and capillary rising. This study adopted the four aforementioned methods, as shown in Figure 1, to comprehensively evaluate the MMP of XH Block crude oil during CO_2 flooding.

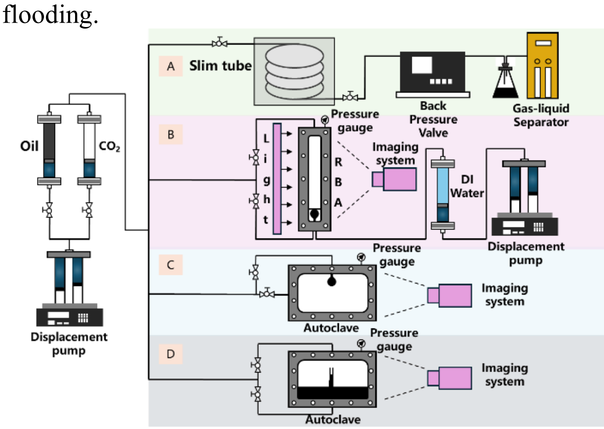

Fig.1 Flow chart of the MMP measurement experimental system: (A) Slim tube method; (B) Bubble rise method; (C) Interfacial tension vanishing method; (D) Capillary rising method.

2.2.1 Slim-tube method

The slim-tube method is widely accepted for measuring the MMP of CO_2-crude oil systems. A one-dimensional sand-packed tube was applied to simulate CO_2 flooding. Under designed temperature and pressure, CO_2 repeatedly contacts crude oil in the tube; adequate mass transfer helps achieve miscibility and increases oil displacement efficiency above 90%. By adjusting displacement pressure to alter miscibility, the displacement efficiency versus pressure curve can be plotted, and the inflection point is defined as MMP [41].

The experimental setup of the slim-tube method is shown in Figure 1(A). The experimental procedures are as follows: ① Stabilize the system at testing conditions, then the slim-tube model is fully saturated with crude oil, where the injected volume needs to be more than 2 hydrocarbon pore volume (HCPV) until the composition of the produced fluid matches that of the original crude oil. ② Inject CO_2 at a constant rate of 0.15 mL/min to displace oil, and record the produced oil/gas volume, composition, phase state, and system pressure as a function of PV injected. ③ Stop the test when cumulative CO_2 injection reaches over 1.2 HCPV. The MMP of the CO_2-oil system is determined to be 13.01 MPa. The detailed results for each displacement are given in Figure 2.

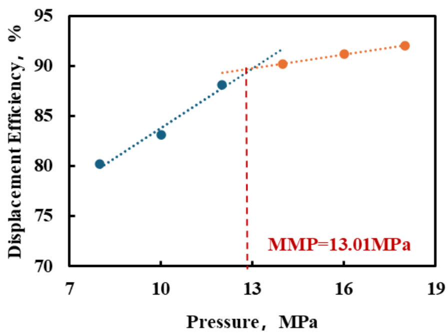

Fig.2 Injection Pressure vs. Recovery Factor.

2.2.2 Bubble rising method

The bubble rising method measures CO_2-crude oil MMP in a vertical crude oil-filled channel, which is also referred to as the rising bubble apparatus (RBA). CO_2 is injected from the bottom of the apparatus. The bubble rising distance and morphology reflect the interphase mass transfer. Then MMP can be determined by observing the migration characteristics of rising CO_2 bubbles. At pressures higher than MMP, CO_2 bubbles can fully dissolve into the crude oil to achieve multiple-contact miscibility [42].

The schematic of the RBA is shown in Figure 1(B). The experimental procedures are as follows: ① Fill the cleaned apparatus with deionized water and pressurize to the designed pressure. ② Inject crude oil from the top to displace water until the oil-water interface is slightly above the needle at the bottom. ③Inject CO_2 to form bubbles with a reasonable size, which rise through the interface into the oil phase under buoyancy. ④Record bubble migration characteristics via photography. The MMP of the CO_2-oil system is determined to be 13.21 MPa. The detailed results are shown in Figure 3.

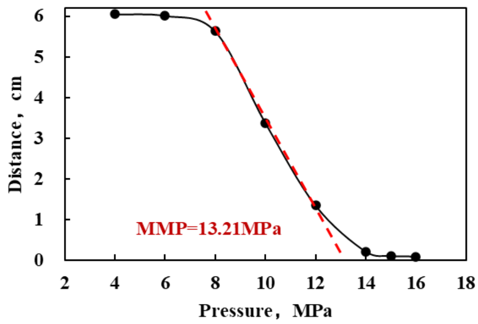

Fig.3 Bubble Rising Distance at Various Pressures.

2.2.3 VIT method

The VIT method is performed in a high-pressure visualized cell. IFT between crude oil and CO_2 is acquired by observing morphological changes of oil droplets in CO_2, from which MMP can be extrapolated. The pressure at which a stable oil droplet cannot be formed and the oil-gas interface vanishes is defined as MMP.

The experimental setup for VIT is shown in Figure 1(C). The experimental procedures are as follows: ① Charge the cleaned cell with CO_2 and stabilize the system at testing pressure and temperature. ②Keep crude oil pressure in the accumulator slightly above the testing pressure. ③ Release oil droplets from the top of the cell via a needle. ④ Depict the droplet image, from which the IFT can be calculated. The MMP of the CO_2-oil system is determined to be 13.42 MPa. The detailed results are presented in Figure 4.

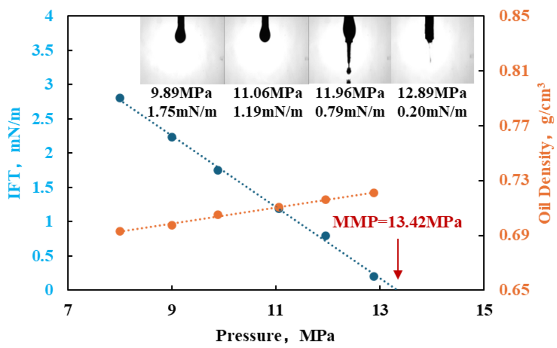

Fig.4 Interfacial Tension Curves of CO_2-XH Crude Oil at Various Pressures.

2.2.4 Capillary rising method

The capillary rising method uses a visualized cell fitted with several fixed capillary tubes. System pressure is adjusted to vary the height of the oil column hight; MMP is defined as the pressure at which the oil column disappears.

The setup is shown in Figure 1(D). The experimental procedures are as follows: ① Evacuate the cleaned cell and stabilize at test temperature. ② Inject crude oil from the bottom of the cell until the oil level is slightly above the bottom of the capillary tube. ③Inject CO_2 from the top of the cell to achieve the desired pressure. ④ Raise pressure stepwise and observe the oil column hight in the capillary tube. The MMP of the CO_2-oil system is determined to be 13.84 MPa. The detailed results are shown in Figure 5.

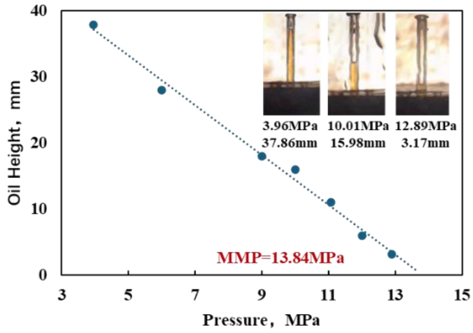

Fig.5 Pressure versus Liquid Level Height.

2.3 Discussion on Comprehensive Evaluation Methods for Miscibility of CO_2-Crude Oil Systems

Table 2 presents the MMP results of the CO_2-XH crude oil system. The slim-tube method yields a lower MMP than the others. As a dynamic displacement process, it achieves multiple-contact miscibility between CO_2 and crude oil. By contrast, the VIT and capillary rising methods are static tests dominated by IFT and capillary force, corresponding to single-contact miscibility and thus resulting in higher MMP. The bubble rising method is semi-dynamic, with its MMP falling between the two categories above.

Table 2. CO_2-XH crude oil system MMP 4 methods comparison.

Number	Method	MMP, MPa
1	Slim-tube	13.01
2	Bubble rising	13.21
3	VIT	13.42
4	capillary rising	13.84

The slim-tube method uses 20 meters one-dimensional sand-packed tube for MMP determination. It realizes continuous CO_2-crude oil interphase mass transfer in porous media, closely simulating field reservoir conditions and possessing high technical maturity. Supported by Chinese industrial standards, it is the most widely used MMP determination method, yet it requires a long test cycle of more than 40 days. The bubble rising method adopts a long visualized one-dimensional cell to directly observe CO_2-oil interphase mass transfer, which undergoes five morphological stages: bubble, bullet, tadpole, jellyfish, and disappearance. With a short test cycle of 1-3 days, it has broad application potential. The VIT and capillary rising methods determine MMP by monitoring pressure-dependent changes in IFT or oil column hight in a high-temperature-high-pressure container. Both methods feature a 1-2 day cycle with good repeatability, showing promising application prospects.

In summary, the four MMP evaluation methods have respective merits. The bubble rising, VIT, and capillary rising methods can be applied to preliminarily constrain the MMP range, laying a basis for precise slim-tube measurement and greatly shortening experimental duration. All four methods are irreplaceable for revealing miscible zone evolution mechanisms. The latter two methods can mutually verify the thermodynamic critical point of miscibility; the slim-tube method reflects the whole propagation process of the miscible zone in porous media; the bubble rising method uniquely captures the full miscibility formation process at the bubble scale, offering key technical support for evaluating miscible zone formation and evolution.

3 Experimental Investigation on Miscible Zone Characteristics in CO_2 Flooding

MMP determination distinguishes CO_2 flooding regimes and facilitates the evaluation of oil-gas miscible zone evolution. Clarifying miscible zone characteristics under miscible, near-miscible, and immiscible flooding is critical for miscible zone regulation and oil recovery enhancement. Controlled by multiple factors, the miscible zone is characterized by leading and trailing propagation, scale variation, and interval phase behaviour.

This study establishes an experimental method to quantitatively investigate the propagation mechanism of miscible zone leading and trailing edges, clarify its scale evolution law, and classify fluid types within its phase interval. The MD is further defined, and a comprehensive miscible zone classification method is proposed. The findings provide fundamental parameters for miscible zone modelling and offer theoretical and technical support for field miscible zone regulation.

3.1 Study on Scale Characteristics of Miscible Zone in CO_2 Flooding

3.1.1 Propagation Boundaries of the Leading and Trailing Edges of the Miscible Zone

Systematic investigation of miscible zone leading and trailing edge propagation clarifies local nonequilibrium evolution and defines oil-gas boundary ranges, laying a basis for quantifying miscible zone scale, phase variation, and spatial distribution, and supplying microscopic support for macroscopic modelling.

This study first incorporates phase and physical properties of the CO_2-oil contact region to define the leading and trailing boundaries of the miscible zone. An experimental evaluation system based on a 20-meter one-dimensional sand-packed tube equipped with online spectroscopy and gas-liquid chromatography was established (Figure 6). A quantitative method was then developed to characterize miscible zone phase behaviour, enabling full-process composition analysis, miscible zone boundary identification, and quantitative interval component characterization.

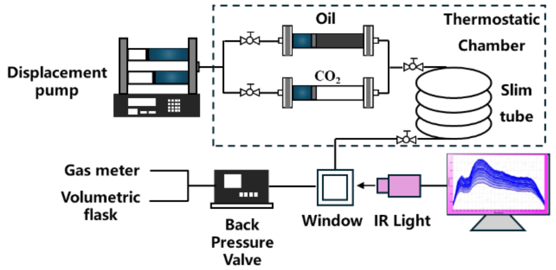

Fig.6 Schematic of Laboratory Evaluation System for CO_2 Flooding.

Using the established evaluation system, long one-dimensional experiments of CO_2 miscible flooding were performed on XH Block crude oil under two conditions: 15 MPa/50 ℃ and 20 MPa/50 ℃, to analyze the evolution of the leading and trailing edges of the miscible zone. At 15 MPa, CO_2 breakthrough occurred at the production end after 0.8 PV injected (Figure 7), while breakthrough took place at only 0.5 PV under 20 MPa, showing a faster leading-edge migration. Higher pressure strengthens CO_2–crude oil mass transfer, accelerates gas migration and advances breakthrough. Moreover, both cases exhibited significant rises in GOR after 0.9 PV injected (Figure 7), accompanied by a gradual increase of the C_2–C_{15} fraction in the produced oil (Figure 8). Although pressure exerts a certain influence on the proportion of heavy fractions, its effect on the trailing edge of the miscible zone is greatly limited when considering the combined factors of gas-oil ratio and the composition of produced fluidto determine the miscible zone trailing edge..

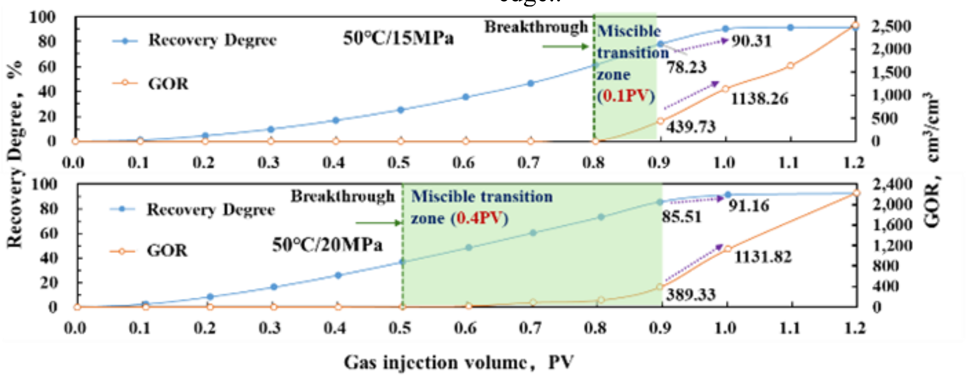

Fig.7 Variation curves of multiphase intervals in miscible zone during CO_2 miscible flooding.

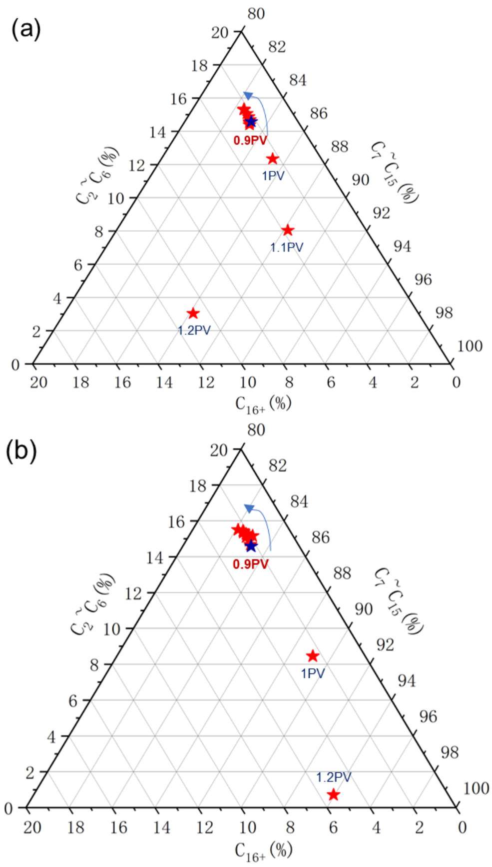

Fig.8 Ternary Phase Diagram for Component Composition of Produced Oil. (a) 15MPa/50℃; (b) 20MPa/50℃.

Key phase parameters were extracted from one-dimensional experiment results to establish a novel criterion for miscible zone boundary division. The miscible zone leading edge is defined by initial CO_2 breakthrough at the production end, while the trailing edge is identified by significant GOR slope rise and increased C_2–C_{15} fractions in the produced oil; the interval between the two boundaries is defined as the miscible zone.

Existing global miscible zone boundary criteria rely on viscosity, swelling factor, MMP, produced fluid composition, and IFT [19,24-25], yet ignore the transition region between the original oil zone and the miscible zone leading edge. Early localization and regulation of the miscible zone are essential for enhancing the recovery by CO_2 flooding. Defining the leading edge via CO_2 breakthrough allows timely identification and regulation, and provides critical engineering parameters for developing miscible zone control technologies to improve oil recovery.

3.1.2 Scale Evolution Law of the Miscible Zone

Based on long one-dimensional physical experiment results, this study systematically identified miscible zone boundaries. Results show that miscible zone length increases with pressure under miscible condition, and oil recovery positively correlates with zone length, rising from 91.56% at 15 MPa to 92.33% at 20 MPa. Since one-dimensional tests cannot visualize miscible regions, a novel CT online scanning system was developed by integrating high-pressure-high-temperature PVT tests with microscopic interface visualization and quantitative CT analysis (Figure 9). This system characterizes CO_2-oil interfacial properties and preliminarily forms a visualized experimental method for miscible zone evaluation.

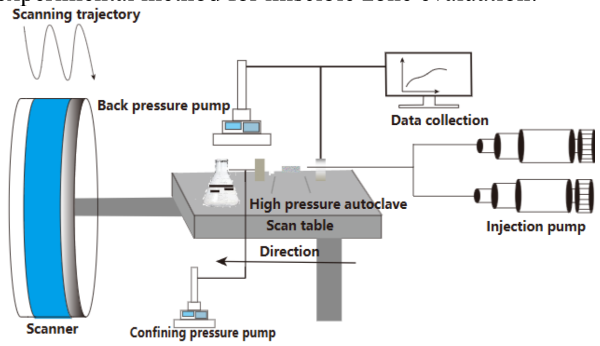

Fig.9 Online CT Scanning Principle and Experimental Flow Diagram.

Given CT values are affected by equipment inherent factors, a full temperature-pressure (100 °C/50 MPa) CT calibration curve for CO_2 was first established (Figure 10), supporting quantitative characterization of CO_2-crude oil miscible zone properties. Combined with dual-energy CT online scanning technology that compromises fluid saturation and core spatial resolution, a rapid pressurization test of the CO_2-crude oil system was conducted in a high-pressure autoclave, and a CT-simulated PVT evaluation method was proposed for the gas-oil mass transfer and miscible process. Experimental results indicate that the overall scale of the miscible zone grows with pressure. As shown in Figure 11, below the MMP of 14.7 MPa, a 4 MPa pressure rise increases the MD by 0.13; above MMP, the same pressure increment raises the value by 0.17–0.35, an increase of 30.7%–169% relative to the sub-MMP condition. CO_2 miscible flooding also expands the scale of the miscible zone and enhances oil displacement efficiency compared with immiscible flooding. With increasing pressure, the miscible zone evolves sequentially into three stages: CO_2 enrichment, crude oil dilution, and accelerated swelling. The findings lay a solid foundation for analyzing controlling factors, phase evolution, and multiphase interval characteristics of the gas-oil contact region during CO_2 flooding.

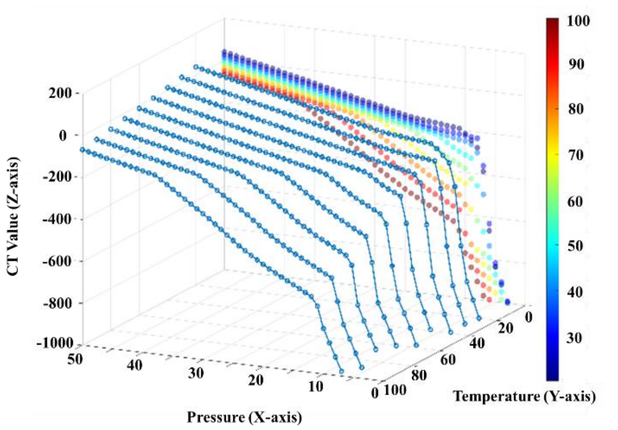

Fig.10 CO_2 Phase Parameters vs. CT Values Correlation Chart.

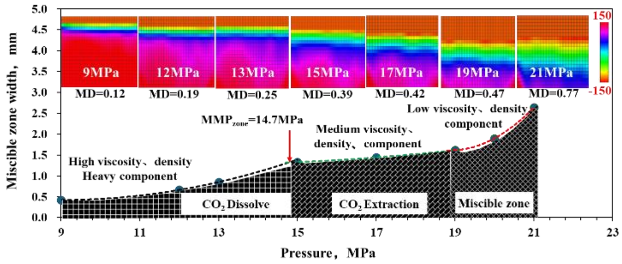

Fig.11 Scale-pressure relationship of oil-gas miscible zone under CO_2 flooding.

3.1.3 Fluid Types in Phase State Intervals of the Miscible Zone

Combined with one-dimensional CO_2 miscible flooding experiment results, the phase transition intervals under 50°C/40 MPa were experimentally evaluated. Based on the GOR of the produced fluid at different displacement stages and the Chinese national standard GB/T 26981, six oil-gas fluid types during CO_2 flooding were preliminarily identified (Figure 12).

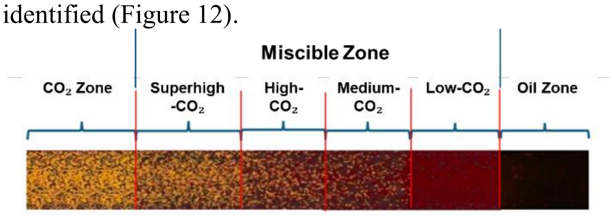

Fig.12 CO_2 Flooding Fluid Type Identification.

Table 3 presents the interval classification of the miscible zone during CO_2 flooding. With the migration and evolution of the miscible zone, six phase intervals are defined: slight CO_2-containing black oil zone, low/medium/high CO_2-containing volatile oil zones, ultra-high CO_2-containing gas condensate zone, and CO_2 main flow zone. According to such divisions, a criterion is preliminarily established to identify fluid types in the multiphase intervals between injection and production wells, laying a theoretical basis for exploring the influencing rules of the multiphase intervals in the miscible zone.

Table 3. Classification of Multi-phase Zones in CO_2 Miscible Displacement.

Fluid Type		Miscible Zone Phase Intervals	Production GOR, m^3/m^3
Wet/Dry Gas		CO_2 Zone	＞2000
Condensate Gas Zone		Superhigh-CO_2 Zone	600~2000
Volatile Oil Zone	Highly Volatile Oil	High-CO_2 Zone	450~600
	Moderately Volatile Oil	Medium-CO_2 Zone	300~450
	Low Volatile Oil	Low-CO_2 Zone	200~300
Black Oil Zone		Oil Zone	30~200

To be noted, different phase intervals have no distinct boundary and fluctuate with gas injection, accompanied by variable interval lengths. Fluid components distribute unevenly within a single interval, with varied oil and gas compositions across regions. Local high-concentration oil or CO_2 zones may form, causing considerable local fluid type changes. Overall, the miscible zone features superposed multiple phase states and presents a spatially gradual mixing zone, where phase intervals transform dynamically in time and space. Clarifying its internal phase evolution provides key guidance for phase regulation, early warning of gas channeling, and gas breakthrough control during CO_2 flooding.

3.2 Formation Mechanism of the Miscible Zone

This study preliminarily clarifies the full-interval phase transition law of CO_2–crude oil systems and reveals the correlations between key factors (IFT, CO_2 concentration, GOR, density, and viscosity) and phase interval evolution during CO_2 miscible flooding. Three flooding patterns are identified: immiscible, near miscible, and miscible, with no clear dividing boundaries among them. Repeated contact between CO_2 and crude oil gradually reduces IFT, enhances mass transfer and diffusion, thus triggering simultaneous condensation and vaporization and forming a dynamically evolving miscible zone. Upon initial contact between CO_2 and original crude oil, equilibrium oil O_{11} and equilibrium gas G_{11} are formed through vaporization-condensation. At this stage, the mobility ratio between equilibrium oil and gas is relatively high; the forward-migrating equilibrium gas G_{11} continues to contact fresh crude oil, forming equilibrium oil O_{12} and equilibrium gas G_{12}. Equilibrium oil O_{11} then contacts pure CO_2, producing equilibrium oil O_{21} and equilibrium gas G_{21} (Figure 13). By analogy, after n cycles of vaporization-condensation between equilibrium gas and equilibrium oil, a special oil-gas region can be formed, which is commonly referred to as the miscible zone.

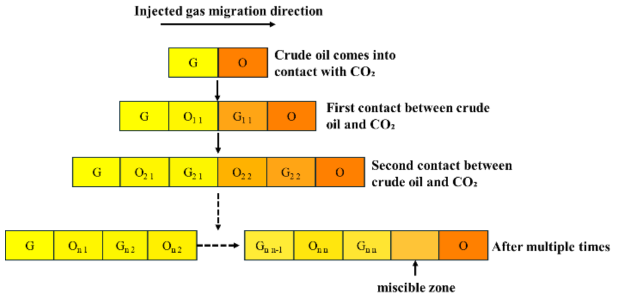

Fig.13 Theoretical Diagram for Microscopic Miscible Zone Generation Mechanism.

At the microscopic scale, the characteristics of the miscible zone are controlled by factors such as oil-gas molecular size, IFT, intermolecular forces, and hydrodynamic dispersion. At the macroscopic scale, it is a function of variables including CO_2 concentration, crude oil type, injection pressure, injection-production well spacing, and reservoir permeability. Driven by both internal and external factors, a special fluid body with a certain spatial range is ultimately formed in the reservoir. In short, the formation of the miscible zone is a process in which the free energy of the two fluids decreases. The free energy calculation is expressed by Equation (1) [45]

$$\frac{\Delta_{mix}G}{RT} = \sum_{j=1}^{N_p}\sum_{i=1}^{N_c}\beta_j x_{ij}\ln\left(\frac{x_{ij}\bar{\phi}_{ij}}{\phi_i}\right) \quad (1)$$

Where: $\Delta_{mix}G$ is the Gibbs free energy change of mixing, R is the universal gas constant, T is the temperature, Np is the number of phases, Nc is the number of components, β is the molar phase fraction, χ is the mole fraction, ϕ is the fugacity coefficient of the pure component, i and j are the component index and phase index, respectively. Driven by the decrease in free energy, gradual miscibility is achieved through mechanisms such as diffusion or interfacial instability. Meanwhile, vaporization-condensation weakens gradually and tends to stabilize (but not vanish) until the miscible zone is fully formed.

3.3 Definition of MD

MD is one of the important indicators for evaluating the enhanced oil recovery by CO_2 flooding. The concept of MD is involved in miscible, near miscible, and immiscible flooding, but its scientific connotation is ambiguous and its influencing factors are complex. Research on MD is still at the initial stage, and few studies have reported its formal definition.

Only Liao et al. [46] proposed that MD is a function of injection pressure and MMP, and gave the calculation formula: $D_{m,inj}=P_{inj}/MMP$, where $D_{m,inj}$ is the MD based on the injection-miscible pressure difference, P_{inj} is the injection pressure. The MD rises with increasing injection pressure, accompanied by a simultaneous increase in oil recovery. However, this method only considers CO_2 miscible flooding and is only applicable when the injection pressure is lower than the miscible pressure; it cannot describe MD under near miscible and immiscible conditions.

By comprehensively evaluating the relationship between reservoir pressure and MMP in different reservoirs of major oilfields in China (Figure 14), the criterion for MD was improved by fully considering both miscible and immiscible flooding, and a new calculation method for MD was proposed, as shown in Equation (2):

$$D_{m,f}=P_f /MMP\times100\% \quad (2)$$

where $D_{m,f}$ is the MD based on reservoir-miscible pressure difference, and P_f is the reservoir pressure.

When reservoir pressure is lower than MMP, $D_{m,f}<1$, and the displacement mode is immiscible CO_2 flooding, the larger the reservoir-miscible pressure difference, the lower the $D_{m,f}$. When reservoir pressure is higher than MMP, $D_{m,f}>1$, and the displacement mode is miscible CO_2 flooding, the larger the reservoir-miscible pressure difference, the higher the $D_{m,f}$.

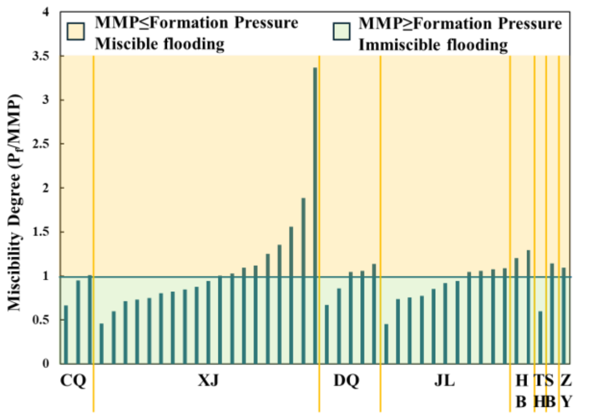

Fig.14 MD chart based on reservoir-miscibility pressure difference.

In addition to the above two pressure-based MD evaluation methods, a calculation method for MD based on visual experimental results was established using CT online scanning experiments of CO_2-crude oil rapid pressurization in a high-pressure cell, as shown in Equation (3).

$$D_{m,CT}=A\_CO_2/A\_oil \tag{3}$$

where $D_{m,CT}$ is the MD based on CT online scanning technology, A_CO2 is the oil-gas contact area, and A_oil is the original oil area. Analysis shows that with increasing pressure, the MD gradually rises from 0.12 to 0.77 (Figure 11).

Based on various experimental types and results, the evaluation of MD should be comprehensively determined by combining multi-parameter, multi-scale, and dynamic evolution characteristics, so as to avoid misjudgment caused by relying on a single index. Therefore, MD calculation method coupling reservoir pressure, MMP, and sweep efficiency is proposed, as shown in Equations (4)-(5).

$$D_m=D_{m,f}\times D_{m,CT}\times L' \tag{4}$$

$$L'=L_{mz,max}/L \tag{5}$$

where D_m is the multi-parameter coupled MD, L' is the miscible zone scale parameter, $L_{mz,max}$ is the maximum distance between the leading and trailing edges of the miscible zone during CO_2 flooding, and L is the injection-production well spacing. The $L_{mz,max}$ can be calculated by using pore volume (PV) divided by cross-sectional area of the slim-tube. This method integrates various characteristics of miscible and immiscible flooding, and realizes a universal evaluation of MD in CO_2 flooding.

4 Establishment of a Mathematical Model for the Miscible Zone in CO_2 Flooding

4.1 Mathematical Model of the Miscible Zone in CO_2 Flooding and Its Solution

This section focuses on the formation, propagation, scale identification, and internal phase evolution of the miscible zone during CO_2 miscible flooding. A mathematical model coupling two-phase flow, convection-dispersion mass transfer, dynamic adsorption, and equation-of-state-based phase behavior calculation is established.

During CO_2 miscible flooding, there is no abrupt single miscible interface from the injection end to the production end. Instead, a dynamic transition zone forms, which is jointly governed by multiple contacts between CO_2 and crude oil, component mass transfer, convection-dispersion, adsorption retention, and phase restructuring. Taking one-dimensional core samples or equivalent flow units as research objects, this paper divides the flow domain into a CO_2-enriched zone, a miscible zone, and an unswept crude oil zone.

.

4.1.1 Governing Equations

The saturations of oil and gas phases satisfy the constraint relationship::

$$S_o+S_g=1 \tag{6}$$

Both the oil phase and gas phase are described by Darcy's law:

$$u_\alpha=-\frac{kk_{r\alpha}}{\mu_\alpha}\frac{\partial p}{\partial x},\qquad \alpha=o,g \tag{7}$$

where u_α denotes the phase flow velocity, k represents absolute permeability, $k_{r\alpha}$ stands for relative permeability, μ is phase viscosity, p is pressure. The Corey model is adopted for the oil and gas relative permeabilities:

$$S_g^*=\frac{S_g-S_{gc}}{1-S_{or}-S_{gc}} \tag{8}$$

$$k_{ro}=k_{ro}^0\left(1-S_g^*\right)^{n_o} \tag{9}$$

$$k_{rg}=k_{rg}^0\left(S_g^*\right)^{n_g} \tag{10}$$

The migration of CO_2 in the oil phase is simultaneously governed by convection, dispersion, dissolution mass transfer and rock adsorption retention, and its governing equation can be written as:

:

$$\frac{\partial\left(\phi S_o x_{CO_2}\right)}{\partial t}+\frac{\partial\left(u_o x_{CO_2}\right)}{\partial x}=\frac{\partial}{\partial x}\left(\phi S_o D\frac{\partial x_{CO_2}}{\partial x}\right)+R_m-R_a$$

(11)

where ϕ represents porosity, S_O denotes oil-phase saturation, u_O is the oil-phase flow velocity, x_{CO2} stands for the mole fraction of CO_2 in the oil phase, D refers to the dispersion coefficient, R_m is the dissolution mass transfer term from the gas phase to the oil phase, and R_α denotes the adsorption retention term. The linear driving force form is adopted for the dissolution mass transfer term:

$$R_m=k_mS_g\left(x_{CO_2}^{eq}-x_{CO_2}\right) \tag{12}$$

where k_m denotes the equivalent mass transfer coefficient, and $x_{CO_2}^{eq}$ represents the equilibrium mole fraction of CO_2 in the oil phase under current temperature and pressure. To eliminate the difference in equilibrium solubility capacity of CO_2 under various temperature and pressure conditions, a dimensionless CO_2 concentration is introduced :

$$C_D = \frac{x_{CO_2}}{x_{CO_2}^{eq}}, \qquad 0 \le C_D \le 1 \qquad (13)$$

4.2 Dynamic Adsorption and Phase Behavior Calculation

The adsorption of CO_2 on rock surfaces is described by a first-order kinetic equation:

$$\frac{dq}{dt} = k_a \left(q^{eq} - q\right) \qquad (14)$$

where$q$ is the actual adsorption capacity, q^{eq} represents the equilibrium adsorption capacity, and k_a denotes the adsorption rate constant. The equilibrium adsorption capacity is characterized by the GAB multilayer adsorption model, which allows the adsorption process to be simultaneously affected by temperature, pressure and local CO_2 concentration. This can reflect the physical laws that elevated temperature reduces adsorption capacity while increased pressure enhances adsorption coverage. .

The phase behavior inside the miscible zone is calculated using the Peng-Robinson equation of state :

$$p = \frac{RT}{V-b} - \frac{a}{V(V+b)+b(V-b)} \qquad (15)$$

Within each grid cell, flash calculations based on the PR-EOS are performed to obtain the number of phases, phase compositions and densities. The LBC viscosity model is further utilized to compute fluid viscosity. Meanwhile, the normalized tie-line length (TLL) criterion is introduced to determine whether near-miscible conditions are achieved locally. Accordingly, the model proposed in this work can be summarized as a coupled framework of MMC-ADE-GAB-PR-EOS-TLL-LBC, where MMC refers to multiple-contact propagation, ADE stands for advection-dispersion equation, GAB denotes dynamic multilayer adsorption, PR-EOS represents the Peng-Robinson equation of state, TLL means tie-line length criterion, and LBC corresponds to the Lohrenz-Bray-Clark viscosity model. .

4.3 Numerical Solution Method

The model is solved using a one-dimensional finite volume difference method. The calculation domain is discretized into N uniform grids along the flow direction, and pore volume multiple at injection is adopted as the time marching variable. At each time step, the oil phase viscosity, volume expansion coefficient, equilibrium dissolution capacity, and adsorption parameters are first updated based on the current temperature, pressure, and local CO_2 concentration. Subsequently, the mobilities and fractional flows of oil and gas phases are calculated to solve the gas phase saturation equation. The upwind scheme is applied to handle the CO_2 advection term, and the central difference scheme is used for the dispersion term, with the dissolution, mass transfer term, and adsorption retention term updated synchronously. Finally, the leading edge, trailing edge, spatial width of the miscible zone, and breakthrough PV at the production end are identified according to the dimensionless CO_2 concentration field.

.

5 Field Application Cases

BLX oil pays are in the Jixian Wumishan Formation, featuring pore-vug-fracture reservoir space and dual-porosity structure. Fracture dips ranging from 60° to 90°, with an average porosity of 6.28% and permeability of 106.5 mD. It is a fractured reservoir conating massive bottom-water, with original oil column height of 373m. The initial reservoir pressure temperature are 38.4MPa and 135℃, respectively. Put into production in 1978 after high-yield output from Well M25, the reservoir underwent three development stages: high stable production, rapid decline, and slow decline. After over 40 years of exploitation, it entered the slow decline phase prior to CO_2 flooding; most producers were shut down due to high water cut, with daily oil production of 18t and water cut of 95%. By July 2025, cumulative CO_2 injection reached 220000 tons (0.02 HCPV), with 13 producers online. Field daily liquid production fell from 400t to 254t, daily oil production rose from 18t to 66t, and water cut dropped from 95% to 73%, achieving obvious water cut reduction and oil increment effects (Figure 15).

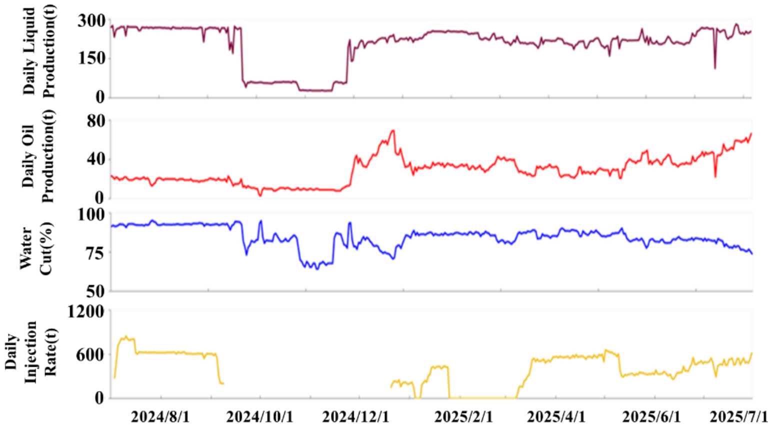

Fig.15 CO_2 injection response and production dynamics of typical wells in BLX reservoir.

The phase behavior variation laws are applied to the BLX reservoir. Combined with field parameters including GOR and produced fluid density, miscible zone migration indicators are established based on fluid type and density, revealing the inter-well miscible zone migration pattern with density as the benchmark (Figure 16). For clarification, Figure 16 uses gas-oil ratio (GOR) to characterize CO_2-oil mixtures via flow similarity analogy, not pure hydrocarbon classification standards. Here, CO_2 is treated as the gas phase and crude hydrocarbons as the liquid phase, with GOR intuitively showing gas-liquid fraction variations across the miscible zone from front to trailing edge. This analogy only helps readers grasp the phase transition trend and does not rigidly classify CO_2-hydrocarbon fluids by pure-oilfield criteria. The figure is merely a qualitative indicator for miscible zone migration stages.

Taking the main producing intervals of the BLX reservoir as the target, time-variant dead oil density curves of typical wells are plotted (Figure 17). M7 and M8 show rising dead oil density with condensate gas fluid, indicating a late miscible zone migration stage. M4 and M5 exhibit declining density and volatile oil characteristics, corresponding to the middle migration stage. M1, M2 and M3 have continuously decreased density and black oil properties, representing the early migration stage. Although M6's dead oil density rises, its heavy component content declines, consistent with M4 and M5, and is thus classified into the middle stage. Overall, in the BLX buried-hill reservoir, 2 wells are in the late miscible zone migration stage, 3 in the middle stage, and 3 in the early stage (Table 5).

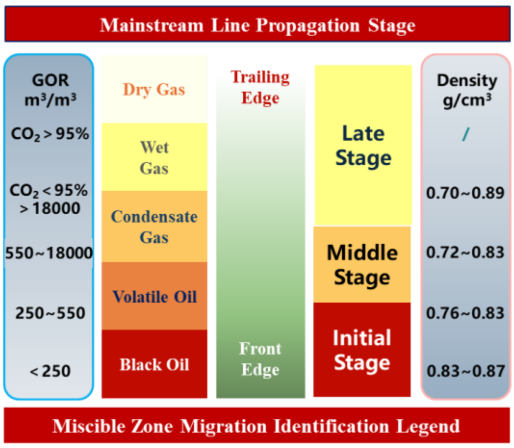

Fig.16 Miscible Zone Migration Identification Legend.

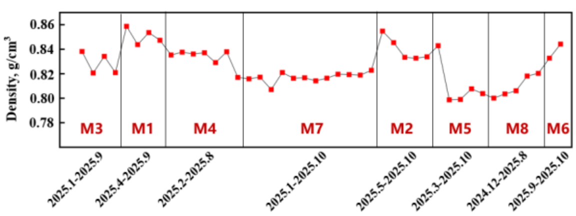

Fig.17 Application Example of BLX.

Table 5. Migration stages and key parameters of miscible zone in different production wells

No.	Location	Fluid type	Density	C_{28+}	Migration stage	Notes
M1	Gas cap miscible zone base	Black oil	↓	↓	Early	Early and middle stages are dominated by displacing original reservoir fluids and extracting fluids with partially dissolved CO_2
M2	Enriched oil belt top/far from gas cap					
M3	Enriched oil belt base					
M4 M5	Gas cap miscible zone base	Volatile oil	↓	↓	Medium	
M6	Enriched oil belt top/close to gas cap					The middle and late stages mainly drive the remaining extracted oil with heavier components.
M7 M8	Gas cap miscible zone top	Condensate gas	↑	↑	Late	

Meanwhile, utilizing the mathematical model for CO_2 miscible zone displacement proposed in this paper, the variation curves of the field GOR over the course of CO_2 injection in the BLX reservoir were simulated and calculated, and comparisons were made with field production data (Figure 18). The results show that the overall agreement between the calculated values from the mathematical model and the field production data is high (>87%). This indicates that the CO_2 displacement mathematical model based on miscible zone characteristics can accurately fit and predict the performance of CO_2 displacement development in the oilfield, effectively supporting the implementation of CO_2 flooding technology and the dynamic adjustment of development plans.

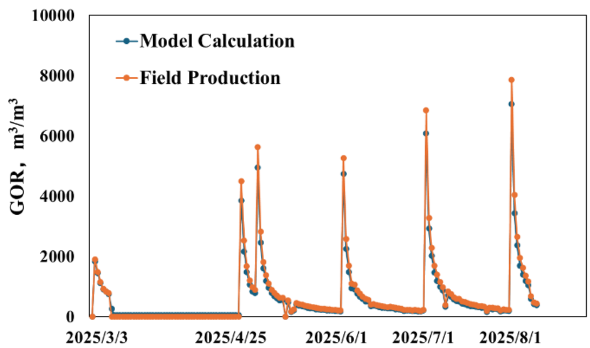

Fig.18 Comparison between simulated GOR results and field production performance of CO_2 flooding in BLX reservoir.

6 Conclusions and suggestions

Aiming at the unclear evolution mechanism of the miscible zone in CO_2 flooding, systematic research was conducted. Four MMP testing methods were compared to summarize a rapid MMP evaluation approach. To unify the inconsistent criteria for miscible zone leading and trailing edges, this study innovatively built a laboratory evaluation system for gas flooding, together with a CT online scanning-based quantitative characterization system for CO_2-crude oil interfacial properties. A boundary discrimination method for the miscible zone was further established, and the variation law of miscible zone scale under key controlling factors was clarified. For the ambiguous internal phase evolution of the miscible zone, a multi-interval phase classification standard was proposed to identify internal oil-gas fluid types, supporting the development of EOR technologies via integrated miscible zone regulation. Based on multiparameter analysis, a definition and calculation method of MD suitable for CO_2 flooding was presented, enabling generalized quantitative miscibility evaluation. Taking the BLX buried-hill reservoir as the field case, miscible zone migration criteria were established, and the interpreted migration characteristics agree well with field data. A dual-mechanism mathematical model coupling seepage and phase behavior for the CO_2 flooding miscible zone was constructed and verified with field production data, laying a solid basis for large-scale application of miscible zone regulation technologies to enhance oil recovery.

To advance targeted and refined development of miscible zone regulation EOR technology for CO_2 flooding, further research is needed on pore-scale miscibility visualization, imaging techniques, and machine learning. Priority should be placed on key technologies, including nanoporous media, three-phase online CT scanning, laser-induced fluorescence, and experiment–simulation interactive digital twin systems. Efficient data analysis and intelligent prediction methods for miscible zone identification and regulation should be established. Real-time data assimilation can continuously update and optimize the miscible zone prediction model, forming a closed-loop verification system integrating laboratory tests, numerical simulation, and field data. This study provides theoretical support for EOR of low/ultra-low permeability reservoirs and efficient development of unconventional oil and gas resources via CO_2 flooding.

References

1. P. Shen, Y. Yang, China Basic Science, **8(3)**, 23 (2006)
2. P. Shen, H. Jiang, Strategic Study of CAE, **11(05)**, 54(2009)
3. S. Yuan, *Gas Injection Enhanced Oil Recovery Technology Collection*, Petroleum Industry Press, 1(2016)
4. T. Fang, M. Wang, J. Li, et al., Industrial & Engineering Chemistry Research, **57(3)**, 1071(2018)
5. Y. Hu, M. Hao, G. Chen, et al., *CO2 Injection Enhanced Oil Recovery Technology*, Petroleum Industry Press, 79, 222(2018)
6. L. Burrows, F. Haeri, P. Cvetic, et al., Energy & Fuels, **34(5)**, 5331(2020)
7. S. Yuan, D. Ma, J. Li, et al., Petroleum Exploration and Development, 49(04), 828(2022)
8. L. Dou, L. Sun, W. Lyu, et al., Petroleum Exploration and Development, **50(5)**, 1083(2023)
9. Y. Hu, W. Lu, Y. Yang, et al., *CO2 Enhanced Oil Recovery and Storage Technology and Practice*, Petroleum Industry Press(2023)
10. X. Song, F. Wang, D. Ma, et al., Petroleum Exploration and Development, **50(01)**, 206(2023)
11. S. Yuan, H. Han, H. Wang, et al., Petroleum Exploration and Development, **51(4)**, 841(2024)
12. Y. Li, Petroleum Geology and Recovery Efficiency, **27(1)**, 1(2020)
13. G. Wang, Petroleum Exploration and Development, **50(01)**, 219(2023)
14. X. Wang, Yanchang Petroleum's Full-Chain Integrated CCUS Technology Progress and Engineering Practice, The 7th International CCUS Forum, Beijing(2023)
15. C. Xiong, S. Li, B. Ding, et al., Chemical Physics Letters, 139044(2021)
16. N. Tileuberdi, I. Gussenov, Energy Reports, **12(12)**, 360(2024)
17. M. Ayoub, B. Tackie-otto, S. Zulkefli, Journal of Petroleum Exploration and Production Technology, **12(11)**, 2899(2022)
18. S. Bachu, J. Shaw, R. Pearson, Proceedings of the SPE/DOE Symposium on Improved Oil Recovery, SPE-89340-MS(2004)
19. S. Li, K. Zhang, D. Ma, et al., Reservoir Evaluation and Development, **5**, 30(2013)
20. R. Syah, S. Alizadeh, M. Nasution, et al., Energy Reports, **7(4)**, 697(2021)
21. S-T. Lee, H. Lo, B. Dharmawardhana, Proceedings of the SPE Annual Technical Conference and Exhibition, SPE-18062-MS(1988)
22. Y. Zhou, R. Wang, F. Gou, et al., Acta Petrolei Sinica, **37(S1)**, 143(2016)
23. Z. Xiao, S. Liu, Y. Li, et al., Petroleum Geology and Recovery Efficiency, **30(2)**, 68(2023)
24. J. Li, Z. Sun, T. Tan, et al., Xinjiang Petroleum Geology, **42(6)**, 714(2021)
25. F. Zhao, M. Zhang, J. Hou, et al., Oilfield Chemistry, **35(04)**, 665(2018)
26. M. Mutailipu, L. Jiang, X. Liu, et al., Fluid Phase Equilibria, **494(1)**, 03(2019)
27. Y. Su, R. Yang, L. Zhang, et al., Processes, **12(4)**, 650(2024)
28. L. Liu, Y. Pi, Y. Liu, et al., IOP Conference Series: Materials Science and Engineering, **768(3)**, 032022(2020)
29. Y. Zhao, Y. Li, G. Fan, et al., Iranian Journal of Chemistry & Chemical Engineering-International English Edition, **41(1)**, 284(2022)
30. F. Orr, K. Jessen, Fluid Phase Equilibria, **255(2)**, 99(2007)
31. M. Cai, Y. Su, Y. Hao, et al., Fuel, **305**,121606(2021)
32. X. Wen, Z. Rui, Y. Zhao, et al., Geoenergy Science and Engineering, **242**, 213284(2024)

33. Y. Luo, S. Yang, Y. Zhang, et al., Processes, **12(6)**, 1203(2024)
34. K. Yang, S. Yang, J. Hu, et al., ACS Omega, **9(28)**, 30131(2024)
35. N. Li, J. Tian, Z. Ren, Oil & Gas Well Testing, **23(04)**, 1(2014)
36. Q. Bo, T. Dai, Y. Yang, Petroleum Drilling Techniques, **44(6)**, 93(2016)
37. Y. Hao, J. Li, C. Kong, et al., Petroleum Science and Technology, **39(21-22)**, 959(2021)
38. X. Cao, Q. Feng, Y. Yang, et al., Oil and gas geology and recovery, **28(1)**,137(2021)
39. Y. Jin, Z. Wang, Z. Zheng, et al., Geosystem Engineering, **26(4)**, 119(2023)
40. J. Li, C. Cui, Z. Wu, et al., Journal of Petroleum Science and Engineering, **218**, 110970(2022)
41. Measurement method for minimum miscibility pressure by slim tube test. SY/T 6573-2016
42. R. Christiansen, H. Haines, SPE Reservoir Engineering, **2(04)**, 523(1987)
43. J. Sievert, J. Dew, F. Conley, Transactions of the AIME, **213(01)**, 228(1958)
44. H. Hao, Study on the formation mechanism and migration law of miscible zone in one-dimensional long-distance CO_2 miscible flooding [Master dissertation, China University of Petroleum, Beijing] (2022)
45. R. Jhalendra, A. Kumar, Fuel, **234**, 770(2018)
46. G. Liao, D. He, G. Wang, et al., Petroleum Exploration and Development, **49(6)**, 1262(2022)